Transport model study of nuclear stopping in heavy-ion collisions over the energy range from 0.09*A* to 160*A* GeV

Ying Yuan,[1,2,*] Qingfeng Li,[3,†] Zhuxia Li,[2,‡] and Fu-Hu Liu[1,§]

[1]*Institute of Theoretical Physics, Shanxi University, Taiyuan, Shanxi 030006, People's Republic of China*

[2]*China Institute of Atomic Energy, Post Office Box 275 (18), Beijing 102413, People's Republic of China*

[3]*School of Science, Huzhou Teachers College, Huzhou, Zhejiang 313000, People's Republic of China*

(Received 1 December 2009; published 30 March 2010)

Nuclear stopping in heavy-ion collisions over a beam energy range from SIS and AGS up to SPS is studied in the framework of the modified Ultrarelativistic Quantum Molecular Dynamics transport model, in which mean field potentials of both formed and "preformed" hadrons (from string fragmentation) and medium-modified nucleon-nucleon elastic cross sections are considered. It is found that nuclear stopping is influenced by both the stiffness of the equation of state and medium modifications of nucleon-nucleon cross sections at SIS energies. At high SPS energies, a two-bump structure is shown in the experimental rapidity distribution of free protons, which can be understood by considering the preformed hadron potentials.

DOI: 10.1103/PhysRevC.81.034913 PACS number(s): 24.10.Lx, 25.75.Dw, 21.65.Mn

I. INTRODUCTION

Since the 1980s heavy-ion collisions (HICs) in terrestrial laboratories have become an important way to investigate properties of hot and dense nuclear matter [1–8]. In particular, the study of transport phenomena in nuclear reactions is of major importance for the understanding of many fundamental properties [9]. And more interest has focused on extracting the equation of state (EoS) of nuclear matter from comparison of microscopic transport models with experimental measurements. Recently, the effect of medium modifications on two-body collisions has received more and more attention.

In one of the attempts to obtain information about the EoS from heavy-ion data [10], it is made clear that progress on this topic requires improved understanding of the momentum dependence of mean fields generated in HICs as well as extensive modification according to experimental information on the degree of stopping achieved [11]. The optimal condition for nuclear matter compressed to form a dense medium is that the two colliding heavy ions are fully stopped by each other during the process of interaction, before the system starts to expand [12]. Information on stopping can be obtained by studying the rapidity distributions of fragments or free nucleons in the transverse and longitudinal directions. In Ref. [11], the ratio of the widths of the transverse to the longitudinal rapidity distributions was proposed to be an indicator of the degree of stopping.

The main purpose of this work is to extract information on nuclear stopping by comparison of the rapidity distributions of protons and other stopping-related observables from a transport-model simulation with data. Meanwhile, medium modifications of interactions of particles in dense matter can be detected as well. This goal can be achieved by studying the excitation function of the stopping from Au + Au collisions at SIS energies and the rapidity distribution of free protons from Au + Au/Pb + Pb collisions at AGS and SPS energies, respectively, within a transport model: the Ultrarelativistic Quantum Molecular Dynamics (UrQMD) model. This method is advantageous (1) to directly compare existing data in each energy region and (2) to minimize uncertainties coming from initial conditions and final freeze-outs when more models are adopted.

II. ULTRARELATIVISTIC QUANTUM MOLECULAR DYNAMICS TRANSPORT MODEL

The UrQMD model is a microscopic many-body transport approach and can be applied to study pp, pA, and AA interactions over an energy range from SIS to RHIC. This transport model is based on the covariant propagation of color strings, constituent quarks, and diquarks (as string ends) accompanied by mesonic and baryonic degrees of freedom [13]. In the present model, the subhadronic degrees of freedom enter via the introduction of a formation time for hadrons produced in the fragmentation of strings [14–16], which are dominant at the early stage of HICs at high SPS and RHIC energies, whereas at SIS and AGS energies, the new particles are produced from the decay of resonances. It is known that, during hadronic transport, two ingredients should be taken carefully into account with if a better comparison with data is needed: mean-field potential and two-body scattering cross section of particles (e.g., Ref. [17]).

A. Mean-field treatments

The UrQMD model is based on parallel principles as the quantum molecular dynamics (QMD) model: hadrons are represented by Gaussian wave packets in phase space and the phase space of hadron i is propagated according to Hamilton's

*wawayubao@sina.com
†liqf@hutc.zj.cn
‡lizwux@ciae.ac.cn
§fuhuliu@163.com

equation of motion [18]:

$$\dot{\vec{r}}_i = \frac{\partial H}{\partial \vec{p}_i}, \dot{\vec{p}}_i = -\frac{\partial H}{\partial \vec{r}_i}. \quad (1)$$

Here $\vec{r}$ and $\vec{p}$ are the coordinate and momentum of the hadron i, respectively. The Hamiltonian H consists of the kinetic energy T and the effective interaction potential energy U,

$$H = T + U. \quad (2)$$

In the standard UrQMD model, the potential energy U includes the two-body and three-body Skyrme, Yukawa, Coulomb, and Pauli terms [18,19],

$$U = U_{\text{sky}}^{(2)} + U_{\text{sky}}^{(3)} + U_{\text{Yuk}} + U_{\text{Cou}} + U_{\text{pau}}. \quad (3)$$

For a better description of experimental data at SIS energies, more potential terms have to be considered [20]. In the modified version of UrQMD (based on version 2.0), the following two terms are added: (1) the density-dependent symmetry potential term U_{sym} and (2) the momentum-dependent term U_{md} [21]. Both the potential terms are very important for the dynamics of intermediate-energy neutron-rich HICs. In this work four parameter sets for the EoS are used for comparison: H-EoS, S-EoS, HM-EoS, and SM-EoS. They are described in Ref. [20].

At higher beam energies (AGS and SPS energies), the Yukawa, Pauli, and symmetry potentials of baryons become negligible, while the Skyrme and the momentum-dependent parts of the potentials still influence the whole dynamical process of HICs [22]. At SPS energies, the new production mechanism of particles (string fragmentation) plays a more and more important role, in which the formation time of hadrons from the string fragmentation is determined by a "yoyo" mode [18,19]. During the formation time, the "preformed" particles (string fragments that will be projected onto hadron states later) are usually treated to be free-streaming, while reduced cross sections are included only for leading hadrons. In previous calculations [18,19,23], the interaction of the newly produced preformed particles is not taken into account. Recently, the mean-field potentials for both formed and preformed particles are considered for a better understanding of the HBT time-related puzzle [24]. Meanwhile, in Ref. [24], the rapidity distribution of net protons from HICs at the SPS energy 158A GeV is shown to have a two-bump structure with consideration of the preformed hadron potentials, which explains the data fairly well. In this paper, more analyses of free protons at all SPS energies are reported.

At AGS and SPS energies, the relativistic effect on the relative distance and the relative momentum and a covariance-related reduced factor used for the update of potentials [22,25] are considered in calculations.

B. In-medium nucleon-nucleon elastic cross sections

Besides the updates of the mean-field part already mentioned, the influence of medium modification on two-nucleon cross sections in the intermediate energy region should also be considered. In the present work we consider medium modifications on NN elastic cross sections in the modified UrQMD model. For inelastic channels, we still use the experimental free-space cross sections. It is believed that this assumption has a minor effect on our present study at SIS energies. At present, three forms of in-medium NN elastic cross sections are considered.

(1) σ^{free}: The free nucleon-nucleon elastic cross section.

(2) $\sigma_1{}^*$: This is based on the extended QHD theory and reads [26,27]

$$\sigma_1{}^* = F(u, \alpha, p)\sigma^{\text{free}}, \quad (4)$$

where the medium correction factor F depends on the nuclear reduced density $u = \rho_i/\rho_0$, the isospin asymmetry $\alpha = (\rho_n - \rho_p)/\rho_i$, and the relative momentum of two colliding nuclei. The ρ_i, ρ_n, and ρ_p are the nuclear, neutron, and proton densities, respectively. More explicitly, the factor F is [26,27]

$$F(u, \alpha, p) = F_u{}^p F_\alpha{}^p, \quad (5)$$

where

$$\begin{cases} F_u{}^p = 1 + \left[\frac{2}{3}\exp(-u/0.54568) - \frac{2}{3}\right]/\left[1 + (p_{NN}/p_0)^\kappa\right], & p_{NN} \leqslant 1\ \text{GeV}/c; \\ F_\alpha{}^p = 1 + \{\tau_{ij}\eta[0.85/(1 + 3.25u)]\alpha\}/[1 + (p_{NN}/p_0)^\kappa], & p_{NN} \leqslant 1\ \text{GeV}/c; \\ F_{\alpha,u}{}^p = 1, & p_{NN} > 1\ \text{GeV}/c. \end{cases} \quad (6)$$

Here p_{NN} is the relative momentum in the NN center-of-mass system; $\tau_{ij} = -1, +1$, and 0 in the case of $i = j = p, i = j = n$, and $i \neq j$, respectively; η is set to -1 for a nonrelativistic-type splitting on proton-proton and neutron-neutron elastic cross sections in the isospin-asymmetric nuclear medium. The other parameters p_0 and κ, which influence the slope of the momentum dependence of the reduction factor F_u, are still somewhat uncertain [27]. In this work, we choose $p_0 = 0.5\ \text{GeV}/c$ and $\kappa = 6$ as an example. Employing this approach, it was found that the in-medium NN elastic cross sections were suppressed more seriously at low relative momenta than at higher ones, depending on the medium density, which is similar to the Brueckner relativistic approach [28,29].

(3) $\sigma_2{}^*$: This is as in Ref. [30] and reads

$$\sigma_2{}^* = (1 - \xi u)\sigma^{\text{free}}, \quad (7)$$

where $\xi = 0.5$ for $E_{\text{lab}} < 0.25A$ GeV in this work. It is easy to find that the momentum constraint is not considered in $\sigma_2{}^*$. Further, the density dependence of $\sigma_2{}^*$ is stronger than that of $\sigma_1{}^*$.

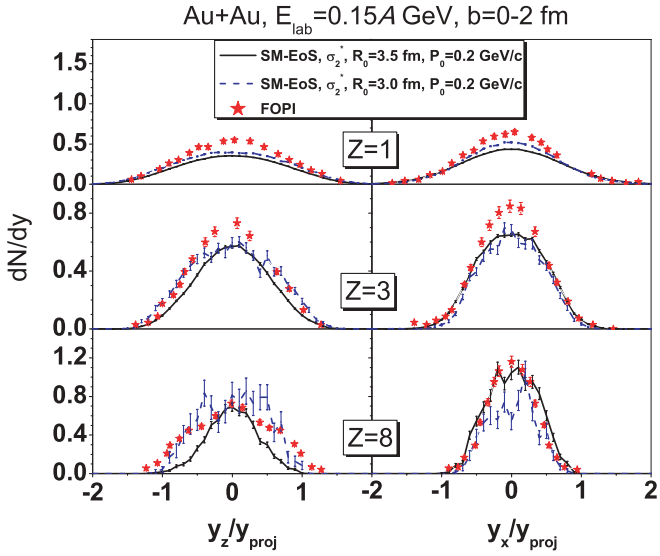

FIG. 1. (Color online) Normalized rapidity distributions of fragments with proton number $Z = 1$, 3, and 8 (from top to bottom) in the longitudinal (left) and transverse (right) directions for central Au + Au collisions at 0.15A GeV. Two (R_0, P_0) parameter sets, (3.5 fm, 0.2 GeV/c) and (3.0 fm, 0.2 GeV/c), are adopted in the coalescence-model calculations, which are shown by lines. FOPI data [12] are represented by stars.

For calculations at SIS, a conventional phase-space coalescence model [31] is used to construct clusters, in which nucleons with relative distances smaller than R_0 and relative momenta smaller than P_0 are considered to belong to one cluster. Figure 1 shows normalized rapidity distributions of fragments with proton number $Z = 1$, 3, and 8 (from top to bottom) in the longitudinal (left) and transverse (right) directions for central Au + Au collisions at 0.15A GeV. Two (R_0, P_0) parameter sets, (3.5 fm, 0.2 GeV/c) and (3.0 fm, 0.2 GeV/c), are adopted in the calculations. The results are shown with lines, and the FOPI data [12] are shown by stars. It seems that the parameter set (3.0 fm, 0.2 GeV/c) gives a better description of the FOPI data. Therefore, this parameter set is used in the following calculations at SIS energies in this work. However, at AGS and SPS energies, the coalescence model is not used as usual (partly because of the rich production of new baryons), so that all nucleons at freeze-out are taken to be free.

III. NUCLEAR STOPPING AND RAPIDITY DISTRIBUTIONS

A. *vartl* at SIS energies

As a measure of the nuclear stopping degree [6], the FOPI Collaboration [11] introduced a new observable *vartl* that is defined by the ratio of the variances of the transverse to the longitudinal rapidity distributions of fragments. For central Au + Au collisions, it is found that the rapidity distributions in the x and y directions are nearly the same, thus the transverse rapidity distributions are plotted approximately with the rapidity distributions in the x direction. Numerically, the *vartl* is defined as

$$vartl = \Gamma_{dN/dy_x}/\Gamma_{dN/dy_z}, \tag{8}$$

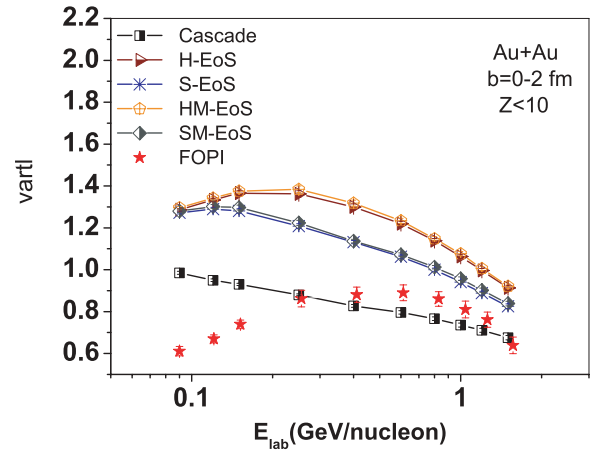

FIG. 2. (Color online) Excitation function of *vartl* for central Au + Au collisions at SIS energies. The FOPI data [11] are shown by stars, while the UrQMD calculations with various EoSs are represented by lines with symbols.

where Γ_{dN/dy_x} (Γ_{dN/dy_z}) is the width of the rapidity distribution of fragments in the x (z) direction and reads

$$\Gamma_{dN/dy_{x,z}} = \sqrt{\langle y_{x,z}^2 \rangle}, \tag{9}$$

$$\langle y_{x,z}^2 \rangle = \frac{\sum \left(y_{x,z}^2 N_{y_{x,z}} \right)}{N_{\rm all}}. \tag{10}$$

Here $N_{y_{x,z}}$ and $N_{\rm all}$ are yields of fragments in each y_x (or y_z) rapidity bin and in the whole rapidity region, respectively. It is easy to understand that $vartl < 1$ stands for an incomplete stopping or nuclear transparency, and $vartl > 1$ for a strong transverse expansion or collectivity. Obviously, $vartl = 1$ when full stopping occurs.

The excitation function of *vartl* for central Au + Au collisions is shown in Fig. 2 within the beam energy region 0.09A–1.5A GeV. The FOPI data [11] are shown by stars, while the UrQMD calculations are shown by lines with symbols. The *vartl* value is calculated for fragments with proton number $Z < 10$. In the calculations, results with the cascade mode and with various EoSs are shown. The free NN cross sections are adopted in the calculations. It is shown that the *vartl* value of the cascade mode is always less than 1 and decreases monotonously with the increase in beam energy, which implies less and less stopping strength in the system. At $E_{\rm lab} \sim 0.3A$–1A GeV calculated values of *vartl* are lower than data. while they are higher than data at lower beam energies. When the mean field is considered, the potentials reinforce the bound of nucleons and stronger collectivity is shown in the transverse direction. Among the calculations with the EoS, a softer EoS gives a smaller *vartl* value, while the momentum-dependent term in the potential plays a negligible role. We also find that only a soft EoS cannot describe the excitation function of the FOPI data without considering medium modifications of two-body collisions. Next, based on the result with the SM-EoS, we further investigate the effect of medium modifications of NN elastic cross sections on the *vartl*.

Figure 3 illustrates the calculated excitation function of *vartl* with the medium-modified NN elastic cross section σ_1^*

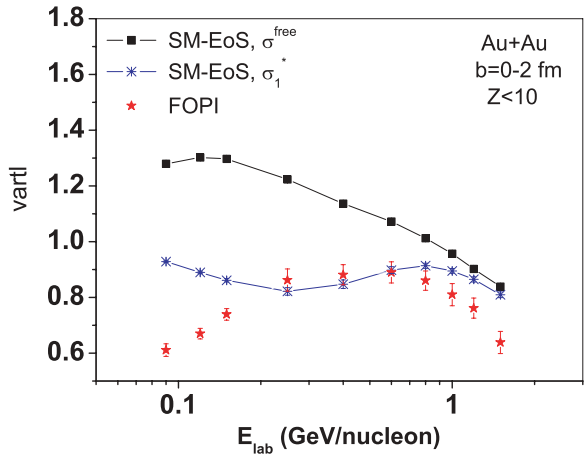

FIG. 3. (Color online) Excitation function of *vartl* with the medium-modified NN elastic cross section $\sigma_1{}^*$ as well as the free one σ^{free}. The SM-EoS was adopted in calculations. FOPI data [11] are shown for comparison.

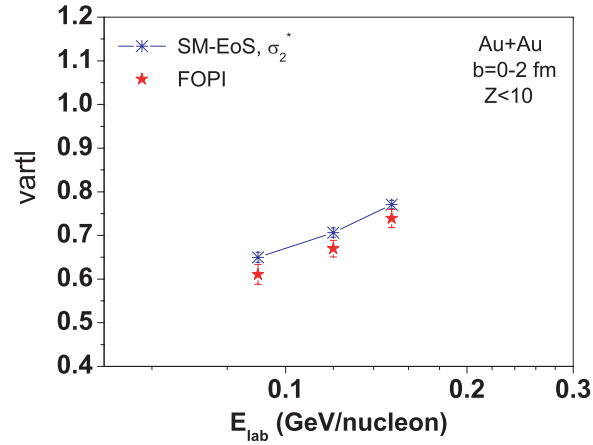

FIG. 4. (Color online) Comparison of the FOPI data [11] with calculations with $\sigma_2{}^*$ for $E_{\text{lab}} < 0.25A$ GeV. The SM-EoS was adopted in calculations.

as well as the free one σ^{free}. It is clearly shown that a large reduction of cross sections at lower beam energies leads to obvious transparency so that the calculated *vartl* values with $\sigma_1{}^*$ are largely decreased at low SIS energies. However, at high SIS energies the *vartl* value is much less affected and slightly higher than the data. As mentioned in Eq. (6), this might be caused by the fixed p_{NN} cut adopted. We would not modify this just for fitting data, as the medium modifications in inelastic channels are still an open question. We just wish to stress the importance of medium modifications of cross sections for nuclear stopping at moderate SIS energies.

For $E_{\text{lab}} < 0.25A$ GeV, the results with $\sigma_1{}^*$ are still higher than the data, which implies that a stronger reduction factor on the elastic cross sections is required. Figure 4 further shows the calculation with $\sigma_2{}^*$ [with a stronger reduction factor on the NN elastic cross section, as shown in Eq. (7)] for $E_{\text{lab}} < 0.25A$ GeV. The comparison with the data is fairly good and the same as done in Ref. [17].

B. Rapidity distribution at AGS and SPS energies

At AGS and SPS energies, as the rapidity distribution of fragments in the transverse direction has not been provided by experiments, we study nuclear stopping with the longitudinal rapidity distribution. Figures 5 and 6 depict the rapidity distributions of protons for central Au + Au collisions at AGS and for central Pb + Pb collisions at SPS (<5% of the total cross section σ_{T}) energies, respectively. The (preliminary) experimental data on free protons are taken from Refs. [32–35]. In the calculations, besides the cascade mode shown at the left, we also show the results with potentials of both formed and "preformed" hadrons ("pf-part & f-B SM-EoS") at the right. Cross sections used in the model are not modified by the nuclear medium in this energy region. Because protons belonging to fragments are included in calculations of the

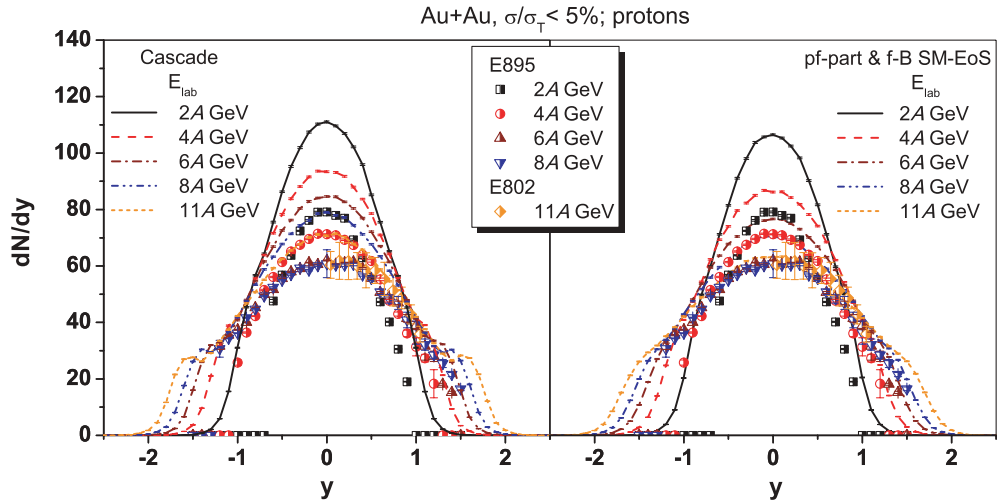

FIG. 5. (Color online) Rapidity distributions of protons at AGS energies 2A, 4A, 6A, 8A, and 11A GeV for central Au + Au collisions. Calculations with cascade (left) and with potentials ("pf-part & f-B SM-EoS"; right) are shown by lines. Experimental data on free protons taken from the E895 [32] and E802 [33] Collaborations are represented by symbols.

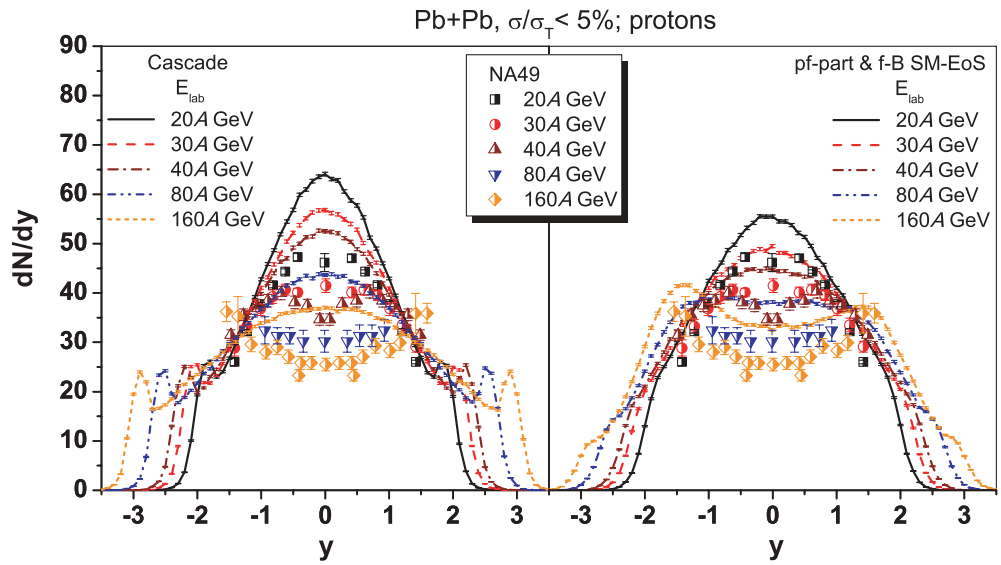

FIG. 6. (Color online) Rapidity distributions of protons at SPS energies 20A, 30A, 40A, 80A, and 160A GeV for central Pb + Pb collisions. Calculations with cascade (left) and with potentials ("pf-part & f-B SM-EoS"; right) are shown by lines. Preliminary data on free protons taken from the NA49 Collaboration [34,35] are represented by symbols.

rapidity distribution, the calculation results for the proton number are somewhat higher than the data, especially at low beam energies as shown in Figs. 5 and 6 as well as in previous calculations [13,36]. In Fig. 5, it is shown that the shape of the rapidity distributions of measured protons changes from one peak at midrapidity with no shoulder to two shoulders upon an increase in beam energy from 2A to 11A GeV. The cascade calculations always give a Gaussian-like distribution at $y < 1.0$, while calculations with potentials are much closer to the data. With the increase in beam energy from AGS to SPS, the experimental rapidity distribution changes further, to a plateau and, finally, to a two-bump structure. Again, calculations in the cascade mode cannot describe the shape of the rapidity distribution of protons completely. The stronger repulsion in the early stage introduced by potentials makes a wider rapidity distribution of protons in the longitudinal direction [24]. The gap of the two peaks becomes wider with an increase in beam energy. Especially, at 160A GeV the rapidity distribution of protons clearly shows two peaks at $y \sim 1.5$. These features can be reasonably reproduced by the calculations with both the formed and the preformed hadron potentials shown at the right in Fig. 6.

We also calculate the rapidity distribution of emitted Λs for central Pb + Pb collisions at 40A and 160A GeV with and without formed and preformed hadron potentials as shown in Fig. 7. Calculations with and without potentials (lines) are compared to the NA49 data [37] (stars). As for the data, the yields represent the sum $\Lambda + \Sigma^0$. It is clearly shown that calculations with potentials are in good agreement with the data at both beam energies, which is caused by the larger transparency introduced by the strongly repulsive mean field at the early stage. It is known that at the AGS and SPS energies the yields of hyperons are somewhat overestimated in UrQMD cascade calculations using versions earlier than 2.1 [18,19,23], which is also shown in Fig. 7. To solve this problem, alternatively, starting from version 2.1 (and the recently published v2.3), the UrQMD group considers additional high mass resonances that are explicitly produced and propagated in s-channel processes with invariant masses up to $\sqrt{s} < 3$ GeV [23,38]. This treatment leads to a lower yield of strange particles so that a nice agreement with Λ data from central Pb + Pb collisions at SPS energies was also shown in previous calculations [13,38]. Therefore, it deserves much more investigation to understand completely the effects of-mean field potentials and the decay of high mass resonances on, for example, particle production and collective flows, which is in progress.

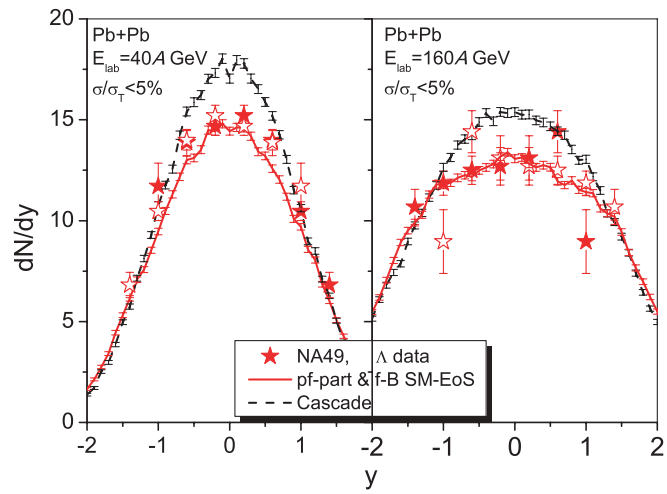

FIG. 7. (Color online) Rapidity distributions of Λ values from central Pb + Pb collisions at 40A GeV (left) and 160A GeV (right). Calculations with and without potentials (lines) are compared to NA49 data [37] (filled stars). Open stars are data points reflected around midrapidity.

IV. SUMMARY AND OUTLOOK

In summary, we have presented the excitation function of the nuclear stopping described by *vartl* of light fragments for central Au + Au reactions with beam energies from $0.09A$ to $1.5A$ GeV and the rapidity distribution of protons and Λs for central Au + Au/Pb + Pb reactions in the energy region $2A$–$160A$ GeV. The modified UrQMD transport model (based on version 2.0) has been used in all calculations. Based on the model we investigate the effects of both mean-field potentials and medium modifications of nucleon-nucleon elastic cross sections on nuclear stopping under the same initial and final freeze-out conditions. It is found that nuclear stopping is influenced by both the stiffness of the EoS and the medium modifications of nucleon-nucleon elastic cross sections for reactions at SIS energies. And it reaches a well-defined plateau of maximal stopping centered around $(0.5 \pm 0.3)A$ GeV, with a fast drop on both sides. At AGS and SPS energies, the degree of nuclear stopping decreases continuously. In the high SPS energy region, as the transparency of matter is high, a two-bump structure is shown in the experimental rapidity distribution of free protons in the longitudinal direction. Our calculations show that considering the potentials of both formed and "preformed" hadrons can improve the agreement between calculation results and data. But the form of the potentials is still simple and rough, and further improvement is needed. Work on this aspect is under way.

ACKNOWLEDGMENTS

We acknowledge support from the Frankfurt Center for Scientific Computing (CSC). This work was supported by the Key Project of the Ministry of Education of China under Grant No. 209053, the National Natural Science Foundation of China under Grant Nos. 10675077, 10975095, 10675172, 10875031, 10905021, and 10979023, the National Basic Research Program of China under Grant No. 2007CB209900, and the Natural Science Foundation of Zhejiang Province under Grant No. Y6090210.

[1] J. Randrup, Nucl. Phys. A **314**, 429 (1979).
[2] Z. Li *et al.*, Nucl. Phys. A **559**, 603 (1993).
[3] Z. Li *et al.*, J. Phys. G **20**, 1829 (1994).
[4] T. K. Choi, M. Maruyama, and F. Takagi, Phys. Rev. C **55**, 848 (1997).
[5] J. D. Bjorken, Phys. Rev. D **27**, 140 (1983).
[6] Q. Li and Z. Li, Chin. Phys. Lett. **19**, 321 (2002).
[7] H. Petersen, Q. Li, X. Zhu, and M. Bleicher, Phys. Rev. C **74**, 064908 (2006).
[8] P. Danielewicz, B. Barker, and L. Shi, AIP Conf. Proc. **1128**, 104 (2009).
[9] C. Escano-Rodriguez *et al.* (INDRA Collaboration and ALADIN Collaboration), Phys. Rev. C **72**, 051601 (2005).
[10] P. Danielewicz, R. Lacey, and W. G. Lynch, Science **298**, 1592 (2002).
[11] W. Reisdorf *et al.* (FOPI Collaboration), Phys. Rev. Lett. **92**, 232301 (2004).
[12] A. Andronic, J. Lukasik, W. Reisdorf, and W. Trautmann, Eur. Phys. J. A **30**, 31 (2006).
[13] H. Petersen, M. Bleicher, S. A. Bass, and H. Stocker, arXiv:0805.0567 [hep-ph].
[14] B. Andersson, G. Gustafson, and B. Nilsson-Almqvist, Nucl. Phys. B **281**, 289 (1987).
[15] B. Nilsson-Almqvist and E. Stenlund, Comput. Phys. Commun. **43**, 387 (1987).
[16] T. Sjostrand, Comput. Phys. Commun. **82**, 74 (1994).
[17] Y. Zhang, Z. Li, and P. Danielewicz, Phys. Rev. C **75**, 034615 (2007).
[18] S. A. Bass *et al.*, Prog. Part. Nucl. Phys. **41**, 255 (1998).
[19] M. Bleicher *et al.*, J. Phys. G **25**, 1859 (1999).
[20] Q. Li, Z. Li, S. Soff, M. Bleicher, and H. Stoecker, J. Phys. G **32**, 151 (2006).
[21] S. A. Bass, C. Hartnack, H. Stöcker, and W. Greiner, Phys. Rev. C **51**, 3343 (1995).
[22] Q. Li and M. Bleicher, J. Phys. G **36**, 015111 (2009).
[23] E. L. Bratkovskaya *et al.*, Phys. Rev. C **69**, 054907 (2004).
[24] Q. Li, M. Bleicher, and H. Stocker, Phys. Lett. B **659**, 525 (2008).
[25] M. Isse, A. Ohnishi, N. Otuka, P. K. Sahu, and Y. Nara, Phys. Rev. C **72**, 064908 (2005).
[26] Q. Li, Z. Li, S. Soff, M. Bleicher, and H. Stoecker, J. Phys. G **32**, 407 (2006).
[27] Q. Li, C. Shen, and M. Di Toro, arXiv:0908.2825 [nucl-th].
[28] C. Fuchs, A. Faessler, and M. El-Shabshiry, Phys. Rev. C **64**, 024003 (2001).
[29] T. Gaitanos, C. Fuchs, and H. H. Wolter, Phys. Lett. B **609**, 241 (2005).
[30] D. Klakow, G. Welke, and W. Bauer, Phys. Rev. C **48**, 1982 (1993).
[31] H. Kruse, B. V. Jacak, J. J. Molitoris, G. D. Westfall, and H. Stöcker, Phys. Rev. C **31**, 1770 (1985).
[32] J. L. Klay *et al.* (E895 Collaboration), Phys. Rev. Lett. **88**, 102301 (2002).
[33] Y. Akiba *et al.* (E802 Collaboration), Nucl. Phys. A **610**, 139C (1996).
[34] C. Blume (NA49 Collaboration), J. Phys. G **34**, S951 (2007) (private communication).
[35] H. Strobele (NA49 Collaboration), arXiv:0908.2777 [nucl-ex].
[36] W. Reisdorf, Prog. Theor. Phys. Suppl. **140**, 111 (2000).
[37] T. Anticic *et al.* (NA49 Collaboration), Phys. Rev. C **80**, 034906 (2009).
[38] H. Petersen, M. Mitrovski, T. Schuster, and M. Bleicher, Phys. Rev. C **80**, 054910 (2009).